

# LatentKeypointGAN: Controlling GANs via Latent Keypoints

Xingzhe He  
 University of British Columbia  
 Vancouver, Canada  
 xingzhe@cs.ubc.ca

Bastian Wandt  
 University of British Columbia  
 Vancouver, Canada  
 wandt@cs.ubc.ca

Helge Rhodin  
 University of British Columbia  
 Vancouver, Canada  
 rhodin@cs.ubc.ca

## Abstract

Generative adversarial networks (GANs) have attained photo-realistic quality. However, it remains an open challenge of how to best control the image content. We introduce *LatentKeypointGAN*, a two-stage GAN that is trained end-to-end on the classical GAN objective yet internally conditioned on a set of sparse keypoints with associated appearance embeddings that respectively control the position and style of the generated objects and their parts. A major difficulty that we address with suitable network architectures and training schemes is disentangling the image into spatial and appearance factors without domain knowledge and supervision signals. We demonstrate that *LatentKeypointGAN* provides an interpretable latent space that can be used to re-arrange the generated images by re-positioning and exchanging keypoint embeddings, such as combining the eyes, nose, and mouth from different images for generating portraits. In addition, the explicit generation of keypoints and matching images enables a new, GAN-based methodology for unsupervised keypoint detection.

## 1. Introduction

It is a long-standing goal to build generative models that picture the distribution of example images faithfully. While we have come close to photo-realism for well-constrained domains, such as faces, it remains challenging to make this image generation process interpretable and editable. For instance, a latent space that disentangles an image into parts and their appearances would allow us to re-combine and reimagine a generated face interactively and artistically. Several approaches exist for disentangling images into parts [61, 73, 26, 53, 64, 37, 12, 68, 40]. However, almost all of these approaches use autoencoder setups combined with

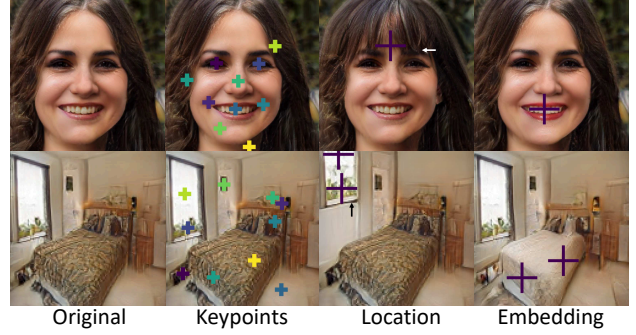


Figure 1. **LatentKeypointGAN** generates high-resolution images (first column) with associated keypoints (second column). These enable localized editing operations, such as moving objects and parts via the respective keypoints (e.g., hair and windows in the third column) or changing the appearance via keypoint embeddings (e.g., mouth and bed in the last column). The arrows show the edited keypoint motion.

equivariance loss functions or augmentation techniques that require careful parameter tuning and yield lower image generation quality.

We propose an alternative approach using GANs that includes keypoints as a latent embedding without requiring any domain knowledge. Although entirely unsupervised, the output of this *LatentKeypointGAN* can subsequently be edited by changing the keypoint position as well as associated appearance embedding locally. A major difficulty that we faced in the absence of keypoint annotations is that high-capacity generators either start ignoring the keypoint locations entirely by conditioning on the noise in early layers that have low spatial resolution or by accounting for keypoint locations but not their noise embedding. The first case defies any semantic editing, and the second prevents

a re-combination of images by exchanging the embeddings of their parts.

LatentKeypointGAN is designed as a two-stage GAN architecture that is trained end-to-end on the standard GAN objective. In the first step, a generator network turns the input noise into 2D keypoint locations and their associated encoding. We ensure with suitable layer connectivity that some of the encodings are correlated while others remain independent. These generated keypoints are then mapped to spatial heatmaps of increasing resolution. The heatmaps define the position of the keypoints and their support sets the influence range of their respective encodings. In the second step, a SPADE-like [47] image generator turns these spatial encodings into a complete and realistic image.

We evaluate the image quality and editing capabilities on a diverse set of image domains: portrait images, human body images, and bedroom images. The chosen GAN architecture yields better image quality compared to existing autoencoder solutions. Although it is not directly applicable for reconstructing, classifying, or modifying existing images, the intermediate keypoint space of LatentKeypointGAN enables us to synthesize a virtually infinite amount of image-keypoint pairs. Albeit not the main motivation of our work, these pairs can be used to train a keypoint detector as a viable alternative to existing unsupervised landmark detection algorithms that rely on autoencoder frameworks.

## 2. Related Work

In the following, we discuss variants of deep generative models that learn to synthesize images from a collection of examples, focusing on methods modeling keypoints and those providing control on the image content.

**GANs** [16] are trained to generate images from a distribution that resembles the training distributions. Recent approaches attain photo-realism for portrait images, e.g., by training a progressive growth of the GAN’s generator and discriminator [29], or by integrating multiplicative neural network layers into StyleGAN [30] and StyleGAN2 [31]. StyleGAN gains some control on the generated high-resolution, high-quality faces, by adopting ideas from style transfer [14, 21] and exchanging features of hidden layers between different samples. More recently, efforts have been made on exploring the latent space of a pre-trained StyleGAN for image editing [52, 25]. Furthermore, to allow editing real-world images, various encoders [75, 1, 2, 17, 65, 50] have been trained to project images into the latent space of StyleGANs. These methods provide control over the image synthesis process, such as for changing age, pose, and gender. To enable rig-like controls over semantic face parameters that are interpretable in 3D, such as illumination, some concurrent researches [59, 58, 15, 9] integrate 3D face models [4, 36] with GANs. Compared with these methods, our model focuses on detailed and local se-

mantic controls. Instead of changing the face as a whole, our method is able to change a local patch without an obvious impact on other regions. Our keypoints provide control handles for animation without manual rigging. Therefore, LatentKeypointGAN can be applied to many different objects and image domains.

**Conditional image synthesis** methods synthesize images that resemble a given reference input, such as category labels [44, 46], text [72, 48], and layout [74, 55]. A variant of the conditional GANs is image-to-image translation [24, 22, 38, 77, 76, 63, 47]. These approaches aim to transfer images from one domain to another while preserving the image structure, such as mapping from day to night. SPADE [47] pioneered using spatially-adaptive normalization to transfer segmentation masks to images, which we borrow and adapt to be conditioned on landmark position. To control individual aspects of faces, such as changing eye or nose shape, recent works condition on segmentation masks [35, 71, 50, 78, 57], rough sketches [62, 6], landmarks [69], or label sets (w/wo glasses, w/wo hat) [7], of faces as input. Closely related to ours is SEAN [78], which conditions on the face segmentation masks with an improved spatially-adaptive normalization to generate high-quality locally controllable face images. Compared with these methods, our model does not take any kind of supervision or other conditions at training time. It is trained in a totally unsupervised manner. Still, our method allows the landmarks to learn a meaningful location and semantic embedding that can be controlled at test time.

**Unsupervised landmark detection** approaches aim to detect the landmarks from images without supervision. Most works [61, 73, 26, 53, 64, 37, 12, 68, 40] train two-branch autoencoders, where shape and appearance are disentangled by training on pairs of images where one of the two is matching while the other factor varies. These pairs can stem from different views [56, 49], from spatial deformation of a source image [61, 67, 73, 60, 37, 8, 12], color shifts [10, 8, 40], and frames of the same video [54, 34, 43, 11, 32, 27]. However, this additional information is not always available or is difficult to capture. Moreover, the parameters of augmentation strategies, such as the thin plate spline deformation model, are difficult to calibrate and lead to unstable training if not. Our GAN approach poses a viable alternative by training a keypoint detector on synthetic examples generated by LatentKeypointGAN.

## 3. LatentKeypointGAN

Our proposed LatentKeypointGAN architecture consists of two sub-networks, the keypoint generator,  $\mathcal{K}$ , and the image generator  $\mathcal{G}$ , which are linked with a spatial embedding layer,  $\mathcal{S}$ . Figure 2 shows the entire architecture. These networks are trained end-to-end on a standard GAN objective, without any supervision on keypoints or masks. At

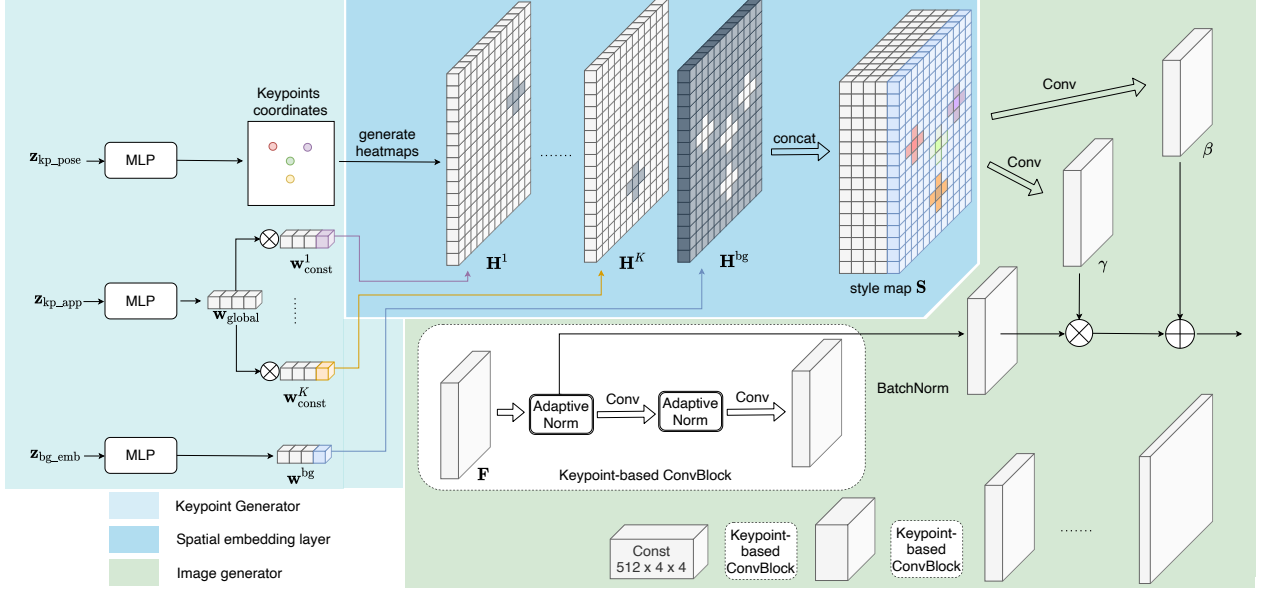


Figure 2. **Overview.** Starting from noise, LatentKeypointGAN generates keypoint coordinates and their embeddings  $\mathbf{w}$ . These are turned into feature maps that are localized around the keypoint and form a conditional map for the image generation via Keypoint-based ConvBlocks.

inference time, the latent keypoints allows one to author the keypoint location and appearance interactively. Moreover, generated keypoint-image pairs can be used to train an independent keypoint detector  $\mathcal{E}$ , thereby mimicking an auto-encoder structure that enables keypoint localization.

The keypoint generator,  $\mathcal{K}$ , is designed to model the spatial arrangement of image parts, such as eyes, nose, and mouth for a portrait image, and their respective local embedding. It takes three Gaussian noise vectors as input  $\mathbf{z}_{\text{kp.pose}}, \mathbf{z}_{\text{kp.app}}, \mathbf{z}_{\text{bg.emb}} \sim \mathcal{N}(\mathbf{0}^{D_{\text{noise}}}, \mathbf{I}^{D_{\text{noise}} \times D_{\text{noise}}})$ , where  $D_{\text{noise}}$  is the dimension. It generates the keypoint positions, keypoint embeddings, and a global background embedding. Section 3.1 explains in detail how we structure  $\mathcal{K}$  to model dependent and independent factors of keypoint appearance, which allows us to model the relations between different parts of the image, e.g., relations between right and left eye color.

The spatial embedding layer,  $\mathcal{S}$ , turns the 2D coordinates of the predicted keypoint locations into discrete style maps that have the same spatial resolution as the feature maps of the generator. They can be seen as a form of a heatmap, with the keypoint embeddings spread around their respective 2D position, thereby controlling local image areas.

The image generator  $\mathcal{G}$  follows the progressively growing architecture of StyleGAN [30], combined with the idea of spatial normalization from SPADE [47], which was designed to generate images conditioned on segmentation masks. In the following, we explain how we replace the role of manually annotated segmentation masks with learned

keypoints.

### 3.1. Keypoint Generator

The keypoint locations are generated with a three-layer MLP followed by a  $\tanh$  activation function to transfer the input noise  $\mathbf{z}_{\text{kp.pose}} \in \mathbb{R}^{D_{\text{noise}}}$  to a vector of length  $2K$ , and reshape it to obtain  $K$  keypoint coordinates  $\mathbf{k}^j \in [-1, 1]^2$ ,  $j = 1, \dots, K$ . The influence range of the keypoints is decided by  $\tau$ . We assume that each keypoint contains the appearance information of a specific part. For example, in face generation, we expect one keypoint to generate variations of eyes and another keypoint to generate different kinds of noses. Based on this assumption, we assign a constant embedding vector  $\mathbf{w}_{\text{const}}^j \in \mathbb{R}^{D_{\text{embed}}}$  to each keypoint  $\mathbf{k}^j$ ,  $j = 1, \dots, K$ . The embeddings are updated during the training but fixed during the testing.

However, if we generate images directly using these constant keypoint embeddings, we will not have control over the keypoint appearance because  $\mathbf{w}_{\text{const}}^j$  is constant over all images. It is equivalent to using a one-hot embedding for the keypoints. We, therefore, introduce a noise-dependent factor to every keypoint that controls variant features. We multiply the constant embedding by a noise vector with a learned covariance matrix. In practice, we use a three-layer MLP to map an independent Gaussian noise  $\mathbf{z}_{\text{kp.app}} \in \mathbb{R}^{D_{\text{noise}}}$  to a global style vector  $\mathbf{w}_{\text{global}} \in \mathbb{R}^{D_{\text{embed}}}$ . Then we do an elementwise multiplication of the global style vector  $\mathbf{w}_{\text{global}}$  and each constant embedding vector  $\mathbf{w}_{\text{const}}^j$ ,

$$\mathbf{w}^j = \mathbf{w}_{\text{global}} \otimes \mathbf{w}_{\text{const}}^j, \quad (1)$$

where  $\otimes$  is the elementwise product, and  $\mathbf{w}^j$  is the final keypoint embedding for keypoint  $j$ .

### 3.2. Spatial Embedding Layer

With keypoint coordinates and embeddings generated, we now turn these point-wise estimates into discrete feature maps that are processed by the convolutional generator. First, we create a heatmap  $\mathbf{H}^j \in \mathbb{R}^{H \times W}$  for each keypoint  $j$  by placing a Gaussian at its location,

$$\mathbf{H}_{y,x}^j = \exp(-\|\mathbf{p} - \mathbf{k}^j\|_2^2/\tau), \quad (2)$$

where  $(y, x) \in \{1, \dots, H\} \times \{1, \dots, W\}$  is the pixel coordinate,  $\mathbf{p} = (2y/H - 1, 2x/W - 1) \in [-1, 1]^2$  is the rescaled pixel coordinate, and  $\tau$  controls the influence range of the keypoints. We also define a heatmap  $\mathbf{H}^{\text{bg}}$  for the background as the negative of all keypoint maps,

$$\mathbf{H}_{y,x}^{\text{bg}} = 1 - \max_j \{\mathbf{H}_{y,x}^j\}_{j=1}^K. \quad (3)$$

Once we have the heatmaps and the keypoint embeddings, we can create the style map  $\mathbf{S} \in \mathbb{R}^{(K+1)D_{\text{embed}} \times H \times W}$ . The style map  $\mathbf{S}$  is the concatenation of the multiplication of the heatmaps with their respective keypoint embedding. Specifically, for each keypoint  $j$ , we replicate keypoint embedding  $\mathbf{w}^j$  at each pixel of the heatmap  $\mathbf{H}^j$  and rescale  $\mathbf{w}^j$  by the heatmap value  $\mathbf{H}_{y,x}^j$  at each pixel  $(y, x)$ ,

$$\mathbf{S}_{c,y,x}^j = \mathbf{H}_{y,x}^j \mathbf{w}_c^j. \quad (4)$$

Here  $c \in \{1, \dots, D_{\text{embed}}\}$  is the index of the channel, and  $\mathbf{S}^j \in \mathbb{R}^{D_{\text{embed}} \times H \times W}$  is a keypoint style map for the  $j$ -th keypoint. The background heatmap is multiplied with the independent noise vector  $\mathbf{w}^{\text{bg}}$  generated from  $\mathbf{z}_{\text{bg,emb}}$  instead of keypoint embedding, but treated equally otherwise. Then we concatenate all  $K$  keypoint style maps  $\{\mathbf{S}^j\}_{j=1}^K$  and the background style map  $\mathbf{S}^{\text{bg}}$  in the channel dimension to obtain the style map  $\mathbf{S}$ . How these style maps are used as conditional variables at different levels of the image generator is explained in the next section.

### 3.3. Image Generator

Our generator starts from a learned  $4 \times 4 \times 512$  constant matrix and keeps applying convolutions and upsampling to obtain the larger and larger feature maps. Following SPADE [47], the original BatchNorm [23] layers are replaced with spatial adaptive normalization [47] to control the content. By contrast to SPADE, we do not condition on annotated segmentation masks but instead on the learned feature maps introduced in sections 3.1, and we do not use the residual links [19] because we found it harmed in combination with progressive training.

To be self-contained, we briefly introduce the spatial adaptive normalization and explain how we use it for our

task. Let  $\mathbf{F}^i \in \mathbb{R}^{N \times C_i \times H_i \times W_i}$  be a  $i$ -th feature map in the network for a batch of  $N$  samples, where  $C_i$  is the number of channels. Here we slightly abuse the notation to denote  $N$  batched style maps of size  $(H_i, W_i)$  as  $\mathbf{S}^i \in \mathbb{R}^{N \times (K+1)D_{\text{embed}} \times H_i \times W_i}$ . The same equation as for BatchNorm [23] is used to normalize the feature map, but now the denormalization coefficients stem from the conditional map, which in our case is the processed style map. Specifically, the resulting value of the spatial adaptive normalization is

$$A_{n,c,y,x}^i(\mathbf{S}, \mathbf{F}) = \gamma_{c,y,x}^i(\mathbf{S}_n^i) \frac{\mathbf{F}_{n,c,y,x}^i - \mu_c^i}{\sigma_c^i} + \beta_{c,y,x}^i(\mathbf{S}_n^i), \quad (5)$$

where  $n \in \{1, \dots, N\}$  is the index of the sample,  $c \in \{1, \dots, C\}$  is the index of channels of the feature map, and  $(y, x)$  is the pixel index. The  $\mu_c^i$  and  $\sigma_c^i$  are the mean and standard deviation of channel  $c$ . The  $\gamma_{c,y,x}^i(\mathbf{S}_n^i)$  and  $\beta_{c,y,x}^i(\mathbf{S}_n^i)$  are the parameters to denormalize the feature map. They are obtained by applying two convolution layers on the style map  $\mathbf{S}_n^i$ .

The generator increases resolution layer-by-layer with multiple adaptive normalization layers, requiring differently-sized feature maps. To create feature maps that match the respective spatial resolution of the generator, we use Equation 2 to create heatmaps with different resolutions.

### 3.4. Loss Functions

**Adversarial losses.** It is crucial for LatentKeypointGAN to use the non-saturating loss [16],

$$\mathcal{L}(\mathcal{G})_{\text{GAN}} = \mathbb{E}_{\mathbf{z} \sim \mathcal{N}} \log(\exp(-\mathcal{D}(\mathcal{G}(\mathbf{z}))) + 1) \quad (6)$$

for the generator, and logistic loss,

$$\mathcal{L}(\mathcal{D})_{\text{GAN}} = \mathbb{E}_{\mathbf{z} \sim \mathcal{N}} \log(\exp(\mathcal{D}(\mathcal{G}(\mathbf{z}))) + 1) + \mathbb{E}_{\mathbf{x} \sim p_{\text{data}}} \log(\exp(-\mathcal{D}(\mathbf{x})) + 1) \quad (7)$$

for the discriminator, with gradient penalty [42] applied only on real data,

$$\mathcal{L}(\mathcal{D})_{\text{gp}} = \mathbb{E}_{\mathbf{x} \sim p_{\text{data}}} \nabla \mathcal{D}(\mathbf{x}). \quad (8)$$

If we replace equation 6, 7 and 8 with the spectral norm [45] and hinge loss [45, 47] used in the original SPADE architecture, we get mostly static, meaningless latent keypoint coordinates. The object part location information is entangled with the key part appearance. The comparison is shown in Figure 3.

**Background loss.** To further disentangle the background and the keypoints, and stabilize the keypoint location, we introduce a background penalty,

$$\mathcal{L}(\mathcal{G})_{\text{bg}} = \mathbb{E}_{\mathbf{z}_1, \mathbf{z}_2} [(1 - \mathbf{H}_1^{\text{bg}}) \otimes \mathcal{G}(\mathbf{z}_1) - (1 - \mathbf{H}_2^{\text{bg}}) \otimes \mathcal{G}(\mathbf{z}_2)], \quad (9)$$



Figure 3. **GAN Loss Importance.** Without gradient penalty + logistic loss, as in SPADE, keypoint coordinates remain static.

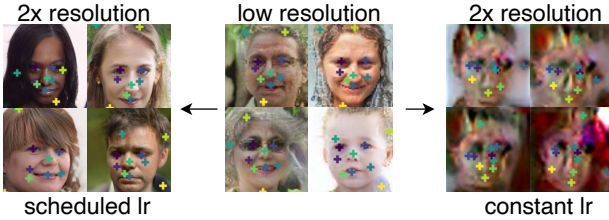


Figure 4. **Scheduling the keypoint generator learning rate.** Reducing the learning rate after each progressive up-scaling step prevents mode collapse and enables high-resolution training.

where  $\mathbf{z}_1$  and  $\mathbf{z}_2$  share the same keypoint location and appearance input noise, and only differ at the background noise input. With this penalty, we expect the keypoint location and appearance do not change with the background.

The final loss for the discriminator is

$$\mathcal{L}(\mathcal{D}) = \mathcal{L}(\mathcal{D})_{\text{GAN}} + \lambda_{\text{gp}} \mathcal{L}(\mathcal{D})_{\text{gp}}, \quad (10)$$

and the total loss for the generator is

$$\mathcal{L}(\mathcal{G}) = \mathcal{L}(\mathcal{G})_{\text{GAN}} + \lambda_{\text{bg}} \mathcal{L}(\mathcal{G})_{\text{bg}}. \quad (11)$$

### 3.5. Progressive Growing Training

We adopt progressive growing training [29] to generate high-resolution images. We tried to train the network end to end following StyleGAN2 [31], MSG-GAN [28], PatchGAN [24], and multi-scale discriminator training [13, 63], but all of them lead to a reduced batch size due to the end-to-end training on high resolution, which is fatal to the training stability, likely due to the BatchNorm that we use in SPADE. We also tried to replace the BatchNorm in SPADE with LayerNorm [3] and PixelNorm [30], but both of them cause mode collapse. On the contrary, the progressive growing training allows for a larger batch size, which helps both on keypoint localization and local appearance learning.

**Keypoint Scheduler.** In the first 40 epochs after changing the resolution, we set the keypoint generator learning rate to zero to fix location and appearance codes. Once the image generator is adapted, we continue training  $\mathcal{K}$ . Otherwise, the keypoint locations diverge and the appearance collapses, as shown in Figure 4.

Following StyleGAN [30], we start from a  $4 \times 4 \times 512$  learned constant matrix, which is optimized during training

and fixed during testing. We use the keypoint-based ConvBlock 2 and bilinear upsampling to obtain feature maps with increasing resolutions. Unlike PGGAN [29] and StyleGAN [30], who generating RGB images from feature maps of all resolutions (from  $4 \times 4$  to  $1024 \times 1024$ ), we start generating RGB images from the feature maps of at least  $64 \times 64$  resolution. It helps to locate the keypoints more accurately.

### 3.6. Keypoint Detector

Although providing editing capability is our main goal, LatentKeypointGAN can generate synthetic image and keypoint pairs. As a side product, it thereby provides an alternative methodology for unsupervised keypoint/landmark detection. To this end, we use a standard keypoint detector architecture in the form of a ResNet [66] that is trained fully supervised on the image-keypoint pairs generated by LatentKeypointGAN. This detector  $\mathcal{E}$  takes an image as input and outputs  $K$  heatmaps, supervised on reference heatmaps generated by Equation 2. It is comparable to the encoder network in autoencoders, with the major difference that it is trained in a post-process. This can be an advantage since independent training can facilitate the higher-capacity encoders used in supervised keypoint detection, and it becomes easier to tune hyperparameters for the reconstruction task instead of jointly for encoding and decoding.

### 3.7. Implementation Details

For all experiments in image generation, we use leaky ReLU [41] with a slope 0.2 for negative values as our activation function. We use ADAM optimizer [33] with  $\beta_1 = 0.5$  and  $\beta_2 = 0.9$ . We set the learning rate to 0.0001 and 0.0004 for generator and discriminators, respectively [20]. We start from generating  $64 \times 64$  images. The batch size for  $64^2, 128^2, 256^2, 512^2$  images are 128, 64, 32, 16, respectively. We set  $\lambda_{\text{gp}} = 10$  and  $\lambda_{\text{bg}} = 100$ .

## 4. Experiments

We evaluate the improved quality and editing operations that our unsupervised LatentKeypointGAN approach for learning disentangled representations brings about. We show the types of edits and high resolution ( $512 \times 512$ ) image generation in Section 4.3 and quantitatively and qualitatively evaluate our image quality compared with other unsupervised and supervised methods in Section 4.4. Although not our main focus, we also evaluate in Section 4.5 the generated keypoint accuracy, comparing LatentKeypointGAN to existing autoencoder frameworks for unsupervised landmark detection.

**Resolution and hyper parameters.** We use  $512 \times 512$  images for face editing,  $256 \times 256$  for human pose experiments, and  $128 \times 128$  for bedroom experiments. Unless specified otherwise, we set  $\tau = 0.01$  and use 10 keypoints.

For experiments on FFHQ and CelebA-HQ, we randomly crop the training images from 70% to 100% to undo the alignment present in these datasets.

## 4.1. Datasets

**CelebA** [39] contains 200k celebrity faces. We use this dataset to test our model’s ability to discover the keypoints unsupervised. Following [61], this dataset is divided into three disjoint sub-datasets, CelebA without MAFL (180k images), MAFL training set (19k images), MAFL test set (1k images). More Details can be found in Section 4.5.

**FlickrFaces-HQ (FFHQ)** [30] consists of 70k high-quality portrait images, with more variation than CelebA [39]. Therefore, we use this dataset to test our model’s ability to disentangle the local representations of images.

**BBC Pose** [5] consists of 20 videos of different sign-language signers with various background. We use this dataset to test our model’s ability to edit human appearance.

**LSUN bedroom** [70] consists of more than 3 million images of bedrooms. We use this dataset to test our model’s generalization ability to edit entire indoor scenes.

## 4.2. Interactive Editing

We show the capabilities of LatentKeypointGAN by changing the keypoint locations and exchanging the keypoint embeddings between different images. As shown in Figure 5, we can change the face direction, face size, and individual key parts by changing the keypoint locations. If only a subset of the keypoint embeddings is changed, the other parts are not significantly affected. Figure 6 shows a heatmap of the area of effect. Since the GAN learns to generate a consistent face from its parts, global effects remain mostly unchanged, for instance, hairstyle and color. We discuss in Section 5 to which degree this is desired and what limitations remain. Additional ablation studies, editing, and interpolation examples are shown in the supplemental document and video.

## 4.3. Disentangled Representations

We first analyze how background and keypoint embeddings are disentangled and used for editing portrait images.

**Disentangled keypoint embeddings.** Figure 6 shows editing operations of independent facial regions. We fix the background noise,  $\mathbf{z}^{\text{bg.emb}}$ , and change some of the keypoint embeddings. This allows to exchanging of eyes, mouth, or nose between persons. Figure 6 includes heatmaps that visualize the difference between original and interpolated images. Their local activation highlights the spatial disentanglement of individual keypoint features.

**Disentangled background.** Figure 7 shows a faithful change of backgrounds while keeping the face fixed. To this end, we fix the keypoint nose  $\mathbf{z}^{\text{key.pos}}$ ,  $\mathbf{z}^{\text{key.emb}}$ , and change

Method	Type	FID score
Pix2PixHD [63]	supervised by masks	23.69
SPADE [47]	supervised by masks	22.43
SEAN [78]	supervised by masks	17.66
Ours	unsupervised, part-based	11.94
StyleGAN [30]	part entangled	5.06

Table 1. **Image quality with respect to supervision type** on CelebA-HQ. Our FID score improves significantly on mask-based solutions while providing similar editing capabilities. It is close to the StyleGAN, which, however, lacks spatially localized editing.

only the background noise input,  $\mathbf{z}^{\text{bg.emb}}$ . The local change in the three diverse examples shows that the background and keypoint encodings are disentangled well.

**Ablation test on the number of keypoints.** By selecting a different number of keypoints, we can achieve different levels of control. In the second row of Figure 8, we use 6 keypoints rather than the default 10. Thereby, keypoints have a smaller area of effect. We observe that the background encoding then takes a larger role and contains the encoding of hair and beard, while the keypoints focus only on the main facial features (nose, mouth, and eyes).

## 4.4. Image Quality

Table 1 shows that compared with segmentation mask-conditioned GANs, our approach attains the lowest FID score of 11.94 on CelebA-HQ. Scores are computed by randomly sampling 50k synthesized images using the Pytorch FID calculator [51]. Figure 9 validates the improved quality, showing greater detail in hair and facial features. Note that Jakab [26] crops images for improved resolution.

## 4.5. Unsupervised Keypoints Discovery

To make a fair comparison, we follow the preprocessing procedure in [73, 61, 26, 40]. We resize all images to  $128 \times 128$  and exclude the training and test set of the MAFL subset from CelebA when training the LatentKeypointGAN. The keypoint detector (defined in Section 3.7) is trained on 200,000 keypoint-image examples generated on the fly by LatentKeypointGAN. Afterward, since the semantic of unsupervised keypoints are undefined, we train a linear regressor from our predicted keypoints to the 5 ground truth keypoints on the MAFL training set, as usual in this protocol. The error is calculated on the MAFL test set as the per-keypoint Euclidean distance between the estimated keypoints normalized by the inter-ocular distance in percent. Our error of 5.85% lies between the 7.95% by Thewlis et al. [61] and the most recent 2.76% by Dundar et al. [12].

LatentKeypointGAN simplifies the existing auto-encoder frameworks by not requiring thin-plate-spline deformation and HSV-color shift layers to encourage disentanglement, which are notoriously difficult to tune.

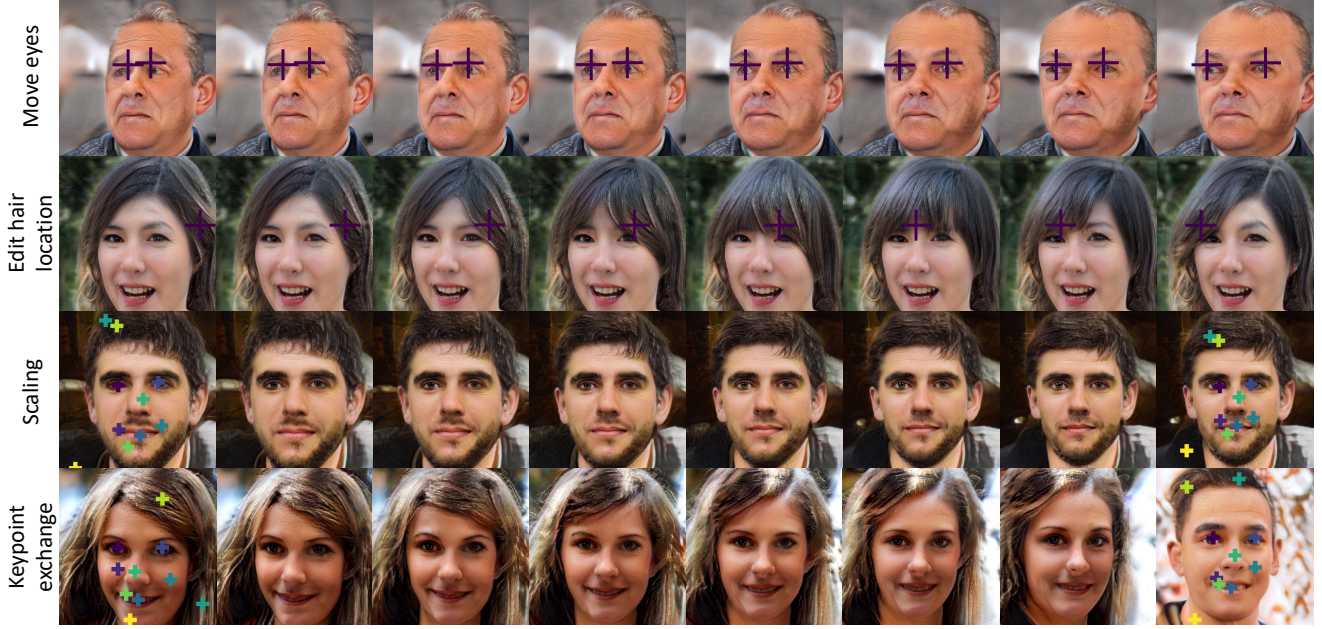


Figure 5. **Location and scale editing.** The first column is the source and the last the target. The images in-between are the result of the following operations. **First row:** pushing the eye keypoint distance from  $0.8x$  to  $1.2x$ . Note that the marked eye keypoints in this row are slightly shifted upward for better visualization. **Second row:** interpolating the hair keypoint to move the fringe from right to left. **Third row:** scaling the keypoint location and, therefore, the face from  $1.15x$  to  $0.85x$ . **Fourth row:** interpolating all keypoint locations, to rotate the head to the target orientation.

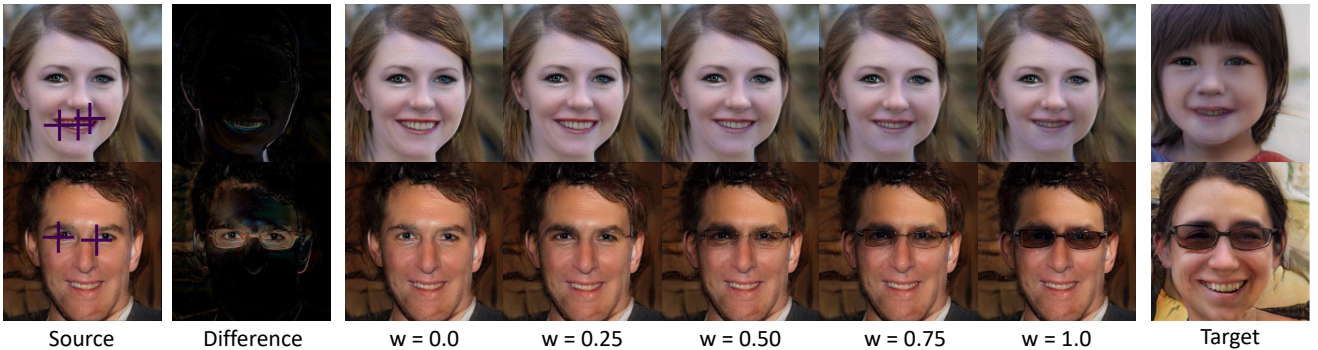


Figure 6. **Disentangled keypoint embeddings** on FFHQ. The leftmost images are the source and the rightmost images are the target. The cross landmarks on the first column denote the parts to be changed. The second column shows the difference between the original image and the changed image. The third to the second to last columns show the interpolation between the original image and the target image.

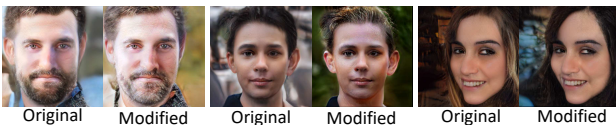


Figure 7. **Disentangled Backgrounds.** The backgrounds are changed while the faces are fixed. The illumination and hair color is learned to be part of the background, which makes sense as a global feature can not be attributed to individual keypoints.

Although LatentKeypointGAN does not exceed the state-of-the-art solutions using autoencoders, it still shows a new methodology to do keypoint detection and exceeds [61]. It is the first step in contesting the existing methodologies.

#### 4.6. Generalization to Other Datasets

**BBC Pose.** Figure 10 explores the editing ability of a person's pose and appearance. Although visual artifacts remain due to the more clear background and blurred humans in the datasets, pose and appearance can be exchanged separately.



Figure 8. **Ablation study** on the number of keypoints. The first row is generated by 10 and the second row by 6 keypoints. More keypoints lead to a stronger influence of the keypoint embedding. However, the 6-keypoint version still provides control, e.g., glasses, nose type, and pose. From left to right: original image, replaced background (difference map overlaid), replaced keypoint embeddings (target image overlaid), exchanged eye embeddings, and keypoint position exchanged.

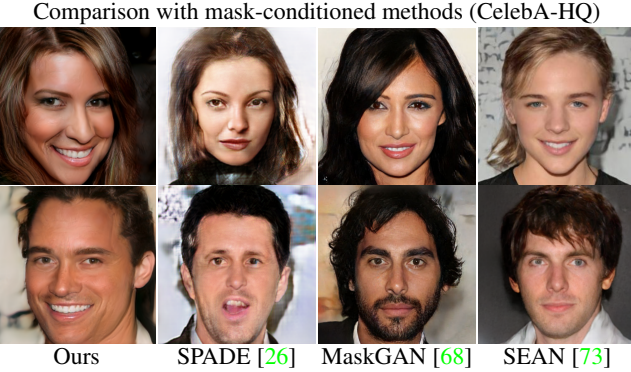


Figure 9. **Image quality comparison.** We compare the image generation quality with both, supervised (top) and unsupervised (bottom). LatentKeypointGAN improves on the methods in both classes.

**LSUN Bedroom.** In Figure 11, we explore the editing ability of entire scenes on the LSUN bedroom dataset. No previous unsupervised part-based model has tried this difficult task before. We successfully interpolate the local appearance by changing the corresponding keypoint embeddings and translating the local key parts (window, bed) by moving the corresponding keypoints. Because our learned representation is 2D it is not possible to rotate objects entirely.



Figure 10. **Editing on BBC Pose.** The first row shows the source image and the second row the editing results. **First two columns:** changing the background (the bottom right corner shows the difference). **middle two columns:** the human appearance is swapped with the small target image. **Fifth column:** changing the position to the one in the overlayed target. **Last column:** the editing results obtained from Lorenz et al. [40] for image quality comparison.

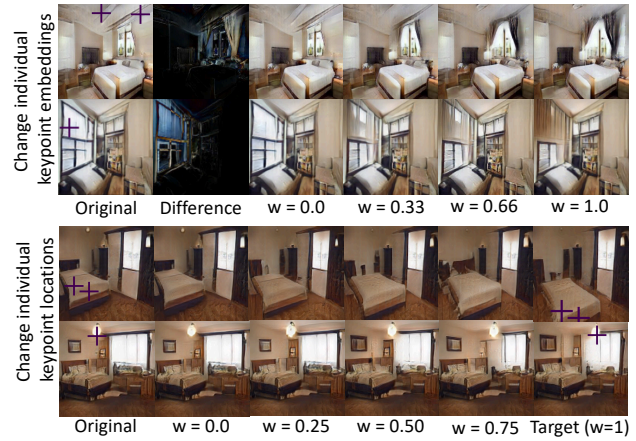


Figure 11. **Editing on Bedroom.** **First row:** interpolating the keypoint embedding on the curtain. **Second row:** interpolating the keypoint embedding on the window. **Third row:** changing the position of keypoint on the bed. **Fourth row:** changing the position of the keypoints on the light.

## 5. Limitations and Future Work

For portrait images, the hair shape and style mixes with the background encoding, yet, the hair can be changed by selecting a background embedding with the desired hair style. Moreover, the disentanglement into locally encoded features can lead to asymmetric faces, such as a pair of glasses with differently styled sides. For BBC Pose, the keypoints are not well localized. They are consistent across images with the same pose, which permits pose transfer, but this proved unsuitable for keypoint detection. Limitations could be overcome by modeling keypoints hierarchically with a skeleton. While the face orientation in portrait images can be controlled, we found that orientation changes on the bedroom images are not reliable. The orientation is often baked into the appearance encoding. We believe that it will be necessary to learn a 3D representation.

It is also worth to mention that LatentKeypointGAN can be trained for a different number of keypoints and scales  $\tau$ , providing fine and coarse-scale control, yet not produce a dynamic number at inference.

## 6. Conclusion

We present a GAN framework that is internally conditioned on keypoints and their appearance encoding, thereby providing an interpretable hidden space that enables intuitive editing. This LatentKeypointGAN also facilitates the generation of image-keypoint pairs, thereby providing a new methodology for unsupervised keypoint detection.

## Acknowledgement

This work was supported in part by the Huawei-UBC Joint Lab project Next Generation 3D Content Creation for End Users on Mobile Devices. Moreover, we thank Farnoosh Javadi and the Hisi Kirin Vision Lab for preparatory work and valuable discussions.

## References

- [1] Rameen Abdal, Yipeng Qin, and Peter Wonka. Image2stylegan: How to embed images into the stylegan latent space? In *Proceedings of the IEEE international conference on computer vision*, pages 4432–4441, 2019. [2](#)
- [2] Rameen Abdal, Yipeng Qin, and Peter Wonka. Image2stylegan++: How to edit the embedded images? In *Proceedings of the IEEE/CVF Conference on Computer Vision and Pattern Recognition*, pages 8296–8305, 2020. [2](#)
- [3] Jimmy Lei Ba, Jamie Ryan Kiros, and Geoffrey E Hinton. Layer normalization. *arXiv preprint arXiv:1607.06450*, 2016. [5](#)
- [4] Volker Blanz and Thomas Vetter. A morphable model for the synthesis of 3d faces. In *Proceedings of the 26th annual conference on Computer graphics and interactive techniques*, pages 187–194, 1999. [2](#)
- [5] James Charles, Tomas Pfister, Derek Magee, David Hogg, and Andrew Zisserman. Domain adaptation for upper body pose tracking in signed tv broadcasts. 2013. [6](#)
- [6] Shu-Yu Chen, Wanchao Su, Lin Gao, Shihong Xia, and Hongbo Fu. Deepfacedrawing: deep generation of face images from sketches. *ACM Transactions on Graphics (TOG)*, 39(4):72–1, 2020. [2](#)
- [7] Yen-Chi Cheng, Hsin-Ying Lee, Min Sun, and Ming-Hsuan Yang. Controllable image synthesis via segvae. In *European Conference on Computer Vision*, 2020. [2](#)
- [8] Zezhou Cheng, Jong-Chyi Su, and Subhransu Maji. Unsupervised discovery of object landmarks via contrastive learning. *arXiv preprint arXiv:2006.14787*, 2020. [2](#)
- [9] Yu Deng, Jiaolong Yang, Dong Chen, Fang Wen, and Xin Tong. Disentangled and controllable face image generation via 3d imitative-contrastive learning. In *IEEE Computer Vision and Pattern Recognition*, 2020. [2](#)
- [10] Xuanyi Dong, Yan Yan, Wanli Ouyang, and Yi Yang. Style aggregated network for facial landmark detection. In *Proceedings of the IEEE Conference on Computer Vision and Pattern Recognition*, pages 379–388, 2018. [2](#)
- [11] Xuanyi Dong, Shou-I Yu, Xinshuo Weng, Shih-En Wei, Yi Yang, and Yaser Sheikh. Supervision-by-registration: An unsupervised approach to improve the precision of facial landmark detectors. In *Proceedings of the IEEE Conference on Computer Vision and Pattern Recognition*, pages 360–368, 2018. [2](#)
- [12] Aysegul Dundar, Kevin J Shih, Animesh Garg, Robert Pottorf, Andrew Tao, and Bryan Catanzaro. Unsupervised disentanglement of pose, appearance and background from images and videos. *arXiv preprint arXiv:2001.09518*, 2020. [1, 2, 6](#)
- [13] Ishan Durugkar, Ian Gemp, and Sridhar Mahadevan. Generative multi-adversarial networks. *International Conference on Learning Representations (ICLR)*, 2016. [5](#)
- [14] Leon A Gatys, Alexander S Ecker, and Matthias Bethge. Image style transfer using convolutional neural networks. In *Proceedings of the IEEE conference on computer vision and pattern recognition*, pages 2414–2423, 2016. [2](#)
- [15] Partha Ghosh, Pravir Singh Gupta, Roy Uziel, Anurag Ranjan, Michael Black, and Timo Bolkart. Gif: Generative interpretable faces. *arXiv preprint arXiv:2009.00149*, 2020. [2](#)
- [16] Ian Goodfellow, Jean Pouget-Abadie, Mehdi Mirza, Bing Xu, David Warde-Farley, Sherjil Ozair, Aaron Courville, and Yoshua Bengio. Generative adversarial nets. In *Advances in neural information processing systems*, pages 2672–2680, 2014. [2, 4](#)
- [17] Shanyan Guan, Ying Tai, Bingbing Ni, Feida Zhu, Feiyue Huang, and Xiaokang Yang. Collaborative learning for faster stylegan embedding. *arXiv preprint arXiv:2007.01758*, 2020. [2](#)
- [18] Kaiming He, Xiangyu Zhang, Shaoqing Ren, and Jian Sun. Delving deep into rectifiers: Surpassing human-level performance on imagenet classification. In *Proceedings of the IEEE international conference on computer vision*, pages 1026–1034, 2015. [13](#)
- [19] Kaiming He, Xiangyu Zhang, Shaoqing Ren, and Jian Sun. Deep residual learning for image recognition. In *Proceedings of the IEEE conference on computer vision and pattern recognition*, pages 770–778, 2016. [4](#)
- [20] Martin Heusel, Hubert Ramsauer, Thomas Unterthiner, Bernhard Nessler, and Sepp Hochreiter. Gans trained by a two time-scale update rule converge to a local nash equilibrium. In *Advances in neural information processing systems*, pages 6626–6637, 2017. [5](#)
- [21] Xun Huang and Serge Belongie. Arbitrary style transfer in real-time with adaptive instance normalization. In *Proceedings of the IEEE International Conference on Computer Vision*, pages 1501–1510, 2017. [2](#)
- [22] Xun Huang, Ming-Yu Liu, Serge Belongie, and Jan Kautz. Multimodal unsupervised image-to-image translation. In *Proceedings of the European Conference on Computer Vision (ECCV)*, pages 172–189, 2018. [2](#)

[23] Sergey Ioffe and Christian Szegedy. Batch normalization: Accelerating deep network training by reducing internal covariate shift. *arXiv preprint arXiv:1502.03167*, 2015. 4

[24] Phillip Isola, Jun-Yan Zhu, Tinghui Zhou, and Alexei A Efros. Image-to-image translation with conditional adversarial networks. In *Proceedings of the IEEE conference on computer vision and pattern recognition*, pages 1125–1134, 2017. 2, 5

[25] Ali Jahanian\*, Lucy Chai\*, and Phillip Isola. On the "steerability" of generative adversarial networks. In *International Conference on Learning Representations*, 2020. 2

[26] Tomas Jakab, Ankush Gupta, Hakan Bilen, and Andrea Vedaldi. Unsupervised learning of object landmarks through conditional image generation. In *Advances in neural information processing systems*, pages 4016–4027, 2018. 1, 2, 6, 8

[27] Tomas Jakab, Ankush Gupta, Hakan Bilen, and Andrea Vedaldi. Self-supervised learning of interpretable keypoints from unlabelled videos. In *Proceedings of the IEEE/CVF Conference on Computer Vision and Pattern Recognition*, pages 8787–8797, 2020. 2

[28] Animesh Karnewar and Oliver Wang. Msg-gan: Multi-scale gradients for generative adversarial networks. In *Proceedings of the IEEE/CVF Conference on Computer Vision and Pattern Recognition*, pages 7799–7808, 2020. 5

[29] Tero Karras, Timo Aila, Samuli Laine, and Jaakko Lehtinen. Progressive growing of gans for improved quality, stability, and variation. In *International Conference on Learning Representations*, 2018. 2, 5, 13

[30] Tero Karras, Samuli Laine, and Timo Aila. A style-based generator architecture for generative adversarial networks. In *Proceedings of the IEEE conference on computer vision and pattern recognition*, pages 4401–4410, 2019. 2, 3, 5, 6, 13

[31] Tero Karras, Samuli Laine, Miika Aittala, Janne Hellsten, Jaakko Lehtinen, and Timo Aila. Analyzing and improving the image quality of stylegan. In *Proceedings of the IEEE/CVF Conference on Computer Vision and Pattern Recognition*, pages 8110–8119, 2020. 2, 5

[32] Yunji Kim, Seonghyeon Nam, In Cho, and Seon Joo Kim. Unsupervised keypoint learning for guiding class-conditional video prediction. In *Advances in Neural Information Processing Systems*, pages 3814–3824, 2019. 2

[33] Diederik P. Kingma and Jimmy Ba. Adam: A method for stochastic optimization. In *International Conference on Learning Representations*, 2015. 5

[34] Tejas D Kulkarni, Ankush Gupta, Catalin Ionescu, Sebastian Borgeaud, Malcolm Reynolds, Andrew Zisserman, and Volodymyr Mnih. Unsupervised learning of object keypoints for perception and control. In *Advances in neural information processing systems*, pages 10724–10734, 2019. 2

[35] Cheng-Han Lee, Ziwei Liu, Lingyun Wu, and Ping Luo. Maskgan: Towards diverse and interactive facial image manipulation. In *Proceedings of the IEEE/CVF Conference on Computer Vision and Pattern Recognition*, pages 5549–5558, 2020. 2

[36] Tianye Li, Timo Bolkart, Michael. J. Black, Hao Li, and Javier Romero. Learning a model of facial shape and expression from 4D scans. *ACM Transactions on Graphics, (Proc. SIGGRAPH Asia)*, 36(6):194:1–194:17, 2017. 2

[37] Weijian Li, Haofu Liao, Shun Miao, Le Lu, and Jiebo Luo. Unsupervised learning of landmarks based on inter-intra subject consistencies. *arXiv preprint arXiv:2004.07936*, 2020. 1, 2

[38] Ming-Yu Liu, Thomas Breuel, and Jan Kautz. Unsupervised image-to-image translation networks. In *Advances in neural information processing systems*, pages 700–708, 2017. 2

[39] Ziwei Liu, Ping Luo, Xiaogang Wang, and Xiaoou Tang. Deep learning face attributes in the wild. In *Proceedings of International Conference on Computer Vision (ICCV)*, December 2015. 6

[40] Dominik Lorenz, Leonard Bereska, Timo Milbich, and Bjorn Ommer. Unsupervised part-based disentangling of object shape and appearance. In *Proceedings of the IEEE Conference on Computer Vision and Pattern Recognition*, pages 10955–10964, 2019. 1, 2, 6, 8

[41] Andrew L Maas, Awni Y Hannun, and Andrew Y Ng. Rectifier nonlinearities improve neural network acoustic models. In *in ICML Workshop on Deep Learning for Audio, Speech and Language Processing*. Citeseer, 2013. 5, 13, 14

[42] Lars Mescheder, Andreas Geiger, and Sebastian Nowozin. Which training methods for gans do actually converge? In *International conference on machine learning*, pages 3481–3490. PMLR, 2018. 4

[43] Matthias Minderer, Chen Sun, Ruben Villegas, Forrester Cole, Kevin P Murphy, and Honglak Lee. Unsupervised learning of object structure and dynamics from videos. In *Advances in Neural Information Processing Systems*, pages 92–102, 2019. 2

[44] Mehdi Mirza and Simon Osindero. Conditional generative adversarial nets. *arXiv preprint arXiv:1411.1784*, 2014. 2

[45] Takeru Miyato, Toshiki Kataoka, Masanori Koyama, and Yuichi Yoshida. Spectral normalization for generative adversarial networks. In *International Conference on Learning Representations*, 2018. 4

[46] Augustus Odena, Christopher Olah, and Jonathon Shlens. Conditional image synthesis with auxiliary classifier gans. In *Proceedings of the 34th International Conference on Machine Learning-Volume 70*, pages 2642–2651, 2017. 2

[47] Taesung Park, Ming-Yu Liu, Ting-Chun Wang, and Jun-Yan Zhu. Semantic image synthesis with spatially-adaptive normalization. In *Proceedings of the IEEE Conference on Computer Vision and Pattern Recognition*, pages 2337–2346, 2019. 2, 3, 4, 6

[48] Scott Reed, Zeynep Akata, Xinchen Yan, Lajanugen Logeswaran, Bernt Schiele, and Honglak Lee. Generative adversarial text to image synthesis. *arXiv preprint arXiv:1605.05396*, 2016. 2

[49] Helge Rhodin, Victor Constantin, Isinsu Katircioglu, Mathieu Salzmann, and Pascal Fua. Neural scene decomposition for multi-person motion capture. In *Proceedings of the IEEE/CVF Conference on Computer Vision and Pattern Recognition (CVPR)*, June 2019. 2

[50] Elad Richardson, Yuval Alaluf, Or Patashnik, Yotam Nitzan, Yaniv Azar, Stav Shapiro, and Daniel Cohen-Or. Encoding

in style: a stylegan encoder for image-to-image translation. *arXiv preprint arXiv:2008.00951*, 2020. 2

[51] Maximilian Seitzer. pytorch-fid: FID Score for PyTorch. <https://github.com/mseitzer/pytorch-fid>, August 2020. Version 0.1.1. 6

[52] Yujun Shen, Jinjin Gu, Xiaouou Tang, and Bolei Zhou. Interpreting the latent space of gans for semantic face editing. In *Proceedings of the IEEE/CVF Conference on Computer Vision and Pattern Recognition*, pages 9243–9252, 2020. 2

[53] Zhixin Shu, Mihir Sahasrabudhe, Riza Alp Guler, Dimitris Samaras, Nikos Paragios, and Iasonas Kokkinos. Deforming autoencoders: Unsupervised disentangling of shape and appearance. In *Proceedings of the European conference on computer vision (ECCV)*, pages 650–665, 2018. 1, 2

[54] Aliaksandr Siarohin, Stéphane Lathuilière, Sergey Tulyakov, Elisa Ricci, and Nicu Sebe. Animating arbitrary objects via deep motion transfer. In *Proceedings of the IEEE Conference on Computer Vision and Pattern Recognition*, pages 2377–2386, 2019. 2

[55] Wei Sun and Tianfu Wu. Image synthesis from reconfigurable layout and style. In *Proceedings of the IEEE International Conference on Computer Vision*, pages 10531–10540, 2019. 2

[56] Supasorn Suwajanakorn, Noah Snavely, Jonathan J Tompson, and Mohammad Norouzi. Discovery of latent 3d keypoints via end-to-end geometric reasoning. In *Advances in neural information processing systems*, pages 2059–2070, 2018. 2

[57] Zhentao Tan, Dongdong Chen, Qi Chu, Menglei Chai, Jing Liao, Mingming He, Lu Yuan, Gang Hua, and Nenghai Yu. Semantic image synthesis via efficient class-adaptive normalization. *arXiv preprint arXiv:2012.04644*, 2020. 2

[58] Ayush Tewari, Mohamed Elgharib, Florian Bernard, Hans-Peter Seidel, Patrick Pérez, Michael Zollhöfer, Christian Theobalt, et al. Pie: Portrait image embedding for semantic control. *arXiv preprint arXiv:2009.09485*, 2020. 2

[59] Ayush Tewari, Mohamed Elgharib, Gaurav Bharaj, Florian Bernard, Hans-Peter Seidel, Patrick Pérez, Michael Zöllhofer, and Christian Theobalt. Stylerig: Rigging stylegan for 3d control over portrait images, cvpr 2020. In *IEEE Conference on Computer Vision and Pattern Recognition (CVPR)*. IEEE, june 2020. 2

[60] James Thewlis, Samuel Albanie, Hakan Bilen, and Andrea Vedaldi. Unsupervised learning of landmarks by descriptor vector exchange. In *Proceedings of the IEEE International Conference on Computer Vision*, pages 6361–6371, 2019. 2

[61] James Thewlis, Hakan Bilen, and Andrea Vedaldi. Unsupervised learning of object landmarks by factorized spatial embeddings. In *Proceedings of the IEEE international conference on computer vision*, pages 5916–5925, 2017. 1, 2, 6, 7

[62] Hung-Yu Tseng, Matthew Fisher, Jingwan Lu, Yijun Li, Vladimir Kim, and Ming-Hsuan Yang. Modeling artistic workflows for image generation and editing. In *European Conference on Computer Vision*, 2020. 2

[63] Ting-Chun Wang, Ming-Yu Liu, Jun-Yan Zhu, Andrew Tao, Jan Kautz, and Bryan Catanzaro. High-resolution image synthesis and semantic manipulation with conditional gans. In *Proceedings of the IEEE conference on computer vision and pattern recognition*, pages 8798–8807, 2018. 2, 5, 6

[64] Wayne Wu, Kaidi Cao, Cheng Li, Chen Qian, and Chen Change Loy. Transgaga: Geometry-aware unsupervised image-to-image translation. In *Proceedings of the IEEE Conference on Computer Vision and Pattern Recognition*, pages 8012–8021, 2019. 1, 2

[65] Jonas Wulff and Antonio Torralba. Improving inversion and generation diversity in stylegan using a gaussianized latent space. *arXiv preprint arXiv:2009.06529*, 2020. 2

[66] Bin Xiao, Haiping Wu, and Yichen Wei. Simple baselines for human pose estimation and tracking. In *European Conference on Computer Vision (ECCV)*, 2018. 5

[67] Xianglei Xing, Ruiqi Gao, Tian Han, Song-Chun Zhu, and Ying Nian Wu. Deformable generator network: Unsupervised disentanglement of appearance and geometry. *arXiv preprint arXiv:1806.06298*, 2018. 2

[68] Yinghao Xu, Ceyuan Yang, Ziwei Liu, Bo Dai, and Bolei Zhou. Unsupervised landmark learning from unpaired data. *arXiv preprint arXiv:2007.01053*, 2020. 1, 2, 8

[69] Xin Yang, Yuezun Li, Honggang Qi, and Siwei Lyu. Exposing gan-synthesized faces using landmark locations. In *Proceedings of the ACM Workshop on Information Hiding and Multimedia Security*, pages 113–118, 2019. 2

[70] Fisher Yu, Ari Seff, Yinda Zhang, Shuran Song, Thomas Funkhouser, and Jianxiong Xiao. Lsun: Construction of a large-scale image dataset using deep learning with humans in the loop. *arXiv preprint arXiv:1506.03365*, 2015. 6

[71] Jun Yu, Xingxin Xu, Fei Gao, Shengjie Shi, Meng Wang, Dacheng Tao, and Qingming Huang. Toward realistic face photo-sketch synthesis via composition-aided gans. *IEEE Transactions on Cybernetics*, 2020. 2

[72] Han Zhang, Tao Xu, Hongsheng Li, Shaoting Zhang, Xiaogang Wang, Xiaolei Huang, and Dimitris N Metaxas. Stackgan: Text to photo-realistic image synthesis with stacked generative adversarial networks. In *Proceedings of the IEEE international conference on computer vision*, pages 5907–5915, 2017. 2

[73] Yuting Zhang, Yijie Guo, Yixin Jin, Yijun Luo, Zhiyuan He, and Honglak Lee. Unsupervised discovery of object landmarks as structural representations. In *Proceedings of the IEEE Conference on Computer Vision and Pattern Recognition*, pages 2694–2703, 2018. 1, 2, 6, 8

[74] Bo Zhao, Lili Meng, Weidong Yin, and Leonid Sigal. Image generation from layout. In *Proceedings of the IEEE Conference on Computer Vision and Pattern Recognition*, pages 8584–8593, 2019. 2

[75] Jiapeng Zhu, Yujun Shen, Deli Zhao, and Bolei Zhou. In-domain gan inversion for real image editing. *arXiv preprint arXiv:2004.00049*, 2020. 2

[76] Jun-Yan Zhu, Taesung Park, Phillip Isola, and Alexei A Efros. Unpaired image-to-image translation using cycle-consistent adversarial networks. In *Proceedings of the IEEE international conference on computer vision*, pages 2223–2232, 2017. 2

[77] Jun-Yan Zhu, Richard Zhang, Deepak Pathak, Trevor Darrell, Alexei A Efros, Oliver Wang, and Eli Shechtman. Toward multimodal image-to-image translation. In *Advances*

*in neural information processing systems*, pages 465–476, 2017. 2

[78] Peihao Zhu, Rameen Abdal, Yipeng Qin, and Peter Wonka. Sean: Image synthesis with semantic region-adaptive normalization. In *Proceedings of the IEEE/CVF Conference on Computer Vision and Pattern Recognition*, pages 5104–5113, 2020. 2, 6

In this appendix, we present additional details on the neural network architectures, the progressive training, and hyperparameters. Furthermore, we show more qualitative results in the supplemental videos that are embedded and explained in our [project website](#).

## A. Keypoints Illustration

In Figure 12, we show the keypoints generated on all datasets.

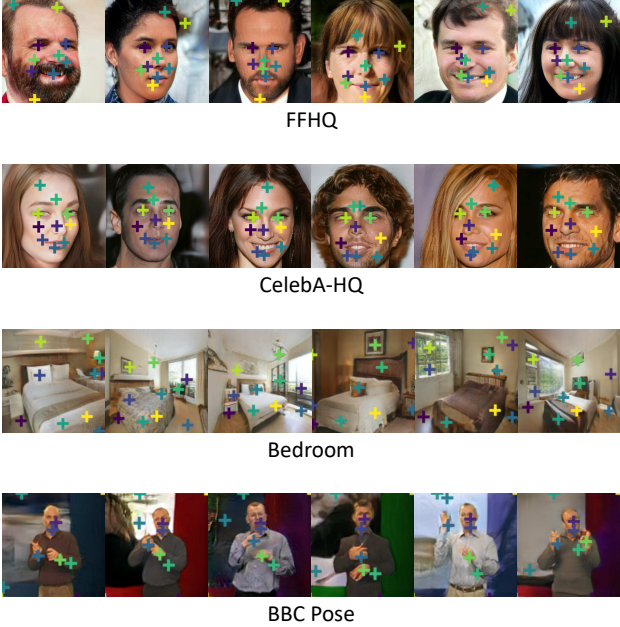


Figure 12. **Keypoints.** We show the keypoints on each dataset.

## B. Experiments Details

**Learning rate and initialization.** We set the learning rate to 0.0001 and 0.0004 for the generator and discriminators, respectively. To let our model learn the coordinates reliably, we first set the learning rate of the MLP, which generates keypoint coordinates to 0.05x the generator learning rate, i.e. 0.00005. We use Kaiming initialization [18] for our network. We initialize the weights of the last layer of the MLP that generates the keypoint coordinates to 0.05x the Kaiming initialization.

**Progressive training.** We use a scheduled learning rate for the Keypoint Generator  $\mathcal{K}$ . As illustrated in Figure 13, at each resolution stage, the training is divided into adapting period and non-adapting period. We set the learning rate of  $\mathcal{K}$  to zero in the adapting period and back to normal in the non-adapting period. In the adapting period, the training follows PGGAN [29] where the feature map is a

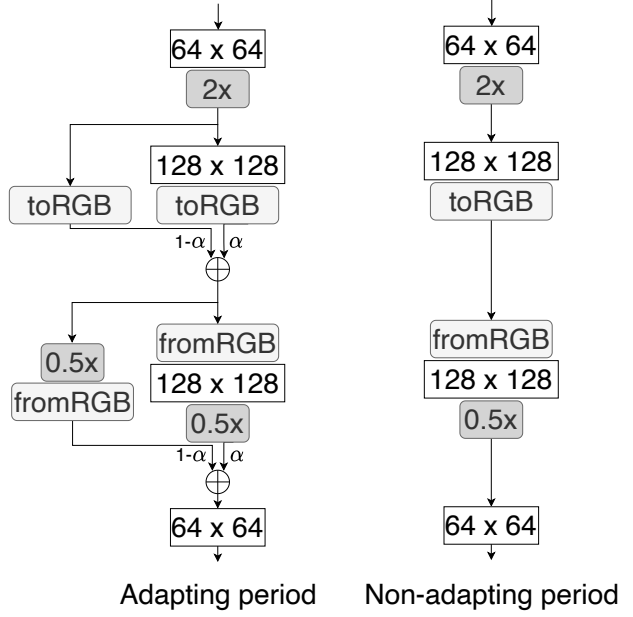


Figure 13. **Progressive training.** The adapting period is the same as PGGAN [29] and StyleGAN [30]. In the non-adapting period, we do not use the linear combination.

linear combination of the larger resolution RGB image and current resolution RGB image. The coefficient  $\alpha$  gradually increases from 0 to 1. At the end of the adapting period, the network is fully adapted to generate higher resolution images. In the non-adapting period, the network generates high-resolution images without the linear combination.

**Generator.** We illustrate the LatentKeypointGAN generator in Figure 14. During the testing time, we only use the last *toRGB* block to generate images.

**Discriminator.** We illustrate the discriminator in Figure 15. For each resolution, we use two convolutions followed by Leaky ReLU [41]. The first convolution has a kernel size  $4 \times 4$  and stride 2 to downsample the feature map to 0.5x. The second convolutions have a kernel size  $3 \times 3$  and stride 1 to extract features.

**Setting for different datasets** We lists the different  $\tau$ s and different background setting for all experiments in Table 2. In CelebA-HQ and FFHQ, the foreground is naturally disentangled from the background. The face can be freely moved on the image. However, in the Bedroom dataset, all objects and their parts are strongly correlated. For example, the bed cannot be moved to the ceiling, and the window cannot be moved to the floor. Therefore, we treat every object in the bedroom as a key part, even the floor, but the possible motion is restricted to plausible locations (see the

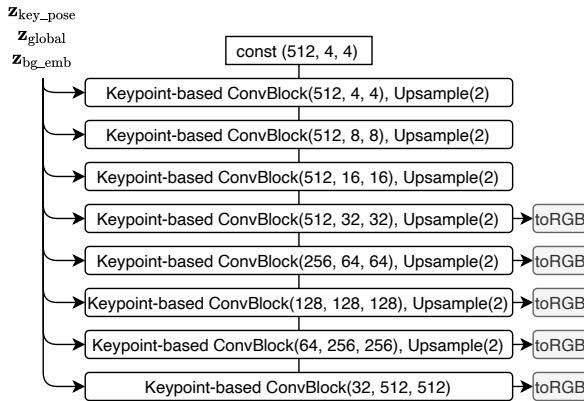


Figure 14. **LatentKeypointGAN generator.** The numbers in the parenthesis is the output dimension of the Keypoint-based ConvBlock. For example, (512, 4, 4) means the output feature map has a resolution of  $4 \times 4$  and the channel size is 512. The toRGB blocks are  $1 \times 1$  convolutions to generate the RGB images with the same resolution as corresponding feature maps.

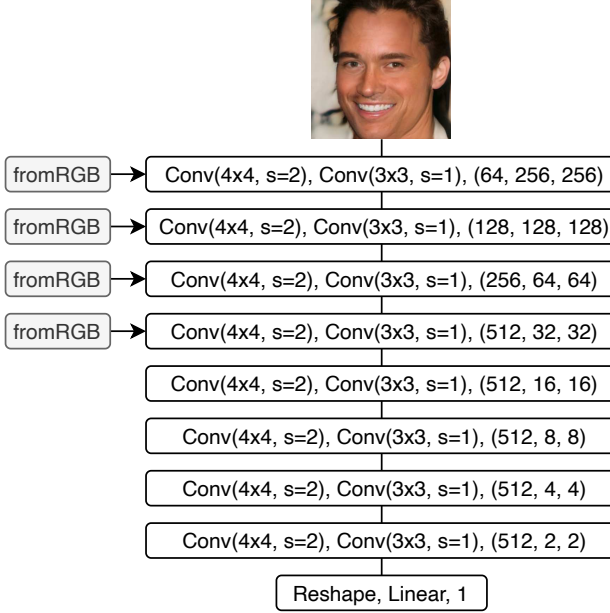


Figure 15. **LatentKeypointGAN discriminator.** The number in the last parenthesis is the output dimension. For example, (512, 4, 4) means the output feature map has a resolution of  $4 \times 4$  and the channel size is 512. At each resolution, we apply two convolutions, one with stride 2 to downsample feature maps and one with stride 1 to extract features. Leaky ReLU [41] is used after all convolutions except the linear layer in the last.

supplementary video). A separate background embedding does not make sense. Therefore, we set the background ( $\mathbf{H}^{bg} = 0$ ) and the background loss  $\lambda_{bg} = 0$  for the experiments on the Bedroom dataset.

Dataset	background module and loss	$\tau$
CelebA-HQ	yes	0.01
FFHQ	yes	0.01
Bedroom	no	0.01
BBC Pose	yes	0.025

Table 2. **Setting for different datasets.** For the Bedroom dataset, we do not use the background module and loss. For the BBC Pose dataset, we use  $\tau = 0.025$ .



Figure 16. **Face generation with on FFHQ with  $\tau = 0.002$ .** We use the red circle to mark the artifacts in the images.



Figure 17. **Failure cases.** The left two images shows asymmetric faces: different eye colors for the man and different blusher for the woman. The last two images shows the entanglement of hair and background.

### C. Ablation Test on $\tau$

A too small value for  $\tau$  does not influence the image and will cause artifacts as shown in Figure 16. A too large value for  $\tau$  will disable the background embedding and control the background.

### D. Failure Cases

As described in the main text, our model sometimes generates asymmetric faces as shown in the first two images in Figure 17. In addition, the hair sometimes is entangled with the background, especially long hair, as shown in the right two images in Figure 17.